

## Accepted Manuscript

Title: Position determination of scatter signatures - a novel sensor geometry

Authors: Anthony Dicken, Keith Rogers, Paul Evans, Joseph Rogers, Jer Wang Chan, Xun Wang



PII: S0039-9140(10)00758-7

DOI: doi:10.1016/j.talanta.2010.09.044

Reference: TAL 11604

To appear in: *Talanta*

Received date: 7-7-2010

Revised date: 6-9-2010

Accepted date: 25-9-2010

Please cite this article as: A. Dicken, K. Rogers, P. Evans, J. Rogers, J.W. Chan, X. Wang, Position determination of scatter signatures - a novel sensor geometry, *Talanta* (2010), doi:10.1016/j.talanta.2010.09.044

This is a PDF file of an unedited manuscript that has been accepted for publication. As a service to our customers we are providing this early version of the manuscript. The manuscript will undergo copyediting, typesetting, and review of the resulting proof before it is published in its final form. Please note that during the production process errors may be discovered which could affect the content, and all legal disclaimers that apply to the journal pertain.

## **Position determination of scatter signatures - a novel sensor geometry**

Anthony Dicken<sup>a\*</sup>, Keith Rogers<sup>a</sup>, Paul Evans<sup>b</sup>, Joseph Rogers<sup>a</sup>,  
Jer Wang Chan<sup>b</sup>, Xun Wang<sup>b</sup>

<sup>a</sup>Department of Translational Medicine, Cranfield Health, Cranfield University,  
Shrivenham, Swindon SN6 8LA, UK

<sup>b</sup>The Imaging Science Group, School of Science and Technology, Nottingham Trent  
University, Nottingham, UK

\*Corresponding author. Tel: +44(0)1793785104; Fax: +44(0)1793783076; E-mail:  
a.dicken@cranfield.ac.uk

### **Abstract**

A novel diffraction sensor geometry able to provide the diffraction pattern of a suspect material without prior knowledge of the samples location is introduced. The sensor geometry can also resolve diffraction patterns originating from multiple unknown materials overlapped along the primary X-ray beam path. This is achieved through tracking Bragg peak maxima that linearly propagate from the inspection volume at a series of X-ray detector positions. A series of simulations and experiments have been performed to verify this technique and provide an insight into its characteristics. Such a technique could have widespread appeal in the security industry. Areas of most relevance include the materials characterisation of volumes such as those prevalent in an airport screening environment or equally the rapid screening for illicit drugs trafficked through the postal system.

Keywords: X-ray diffraction; angular dispersive; ADXRD; security screening;  
explosives; drugs

### **1. Introduction**

A single approach with high sensitivity and specificity that can effectively and non-destructively screen volumes for illicit materials is yet to be adopted by the security industry. Materials that need to be identified include concealed explosives and controlled substances. Explosives are considered by many authors to be the most severe threat to airport security [1], and their perceived presence has placed an unprecedented moral and economic burden on the aviation industry. In the long term the illegal trafficking of controlled substances through the postal system (both domestically and internationally) can be considered equally as detrimental to society.

X-ray diffraction has been shown to be an effective probe for detecting both concealed explosives [2,3,4,5] and controlled substances [6,7,8,9]. These materials are generally of a crystalline nature and therefore produce characteristic diffraction maxima likened to “fingerprints” by some authors [6]. The majority of these proposed screening systems use

an energy dispersive method whereby characteristic X-ray spectra are obtained from individual locations within the inspection volume that is illuminated with a broad-band of radiation. Generally a sophisticated set of collimators which restrict the direction of the incident and diffracted rays is required to ensure that the origin of the scattered radiation (sample position) is well defined. This collimation impinges on the system sensitivity and can result in as much as a 99% loss of the scattered beam flux [4].

We have been investigating a new approach which uses an angular dispersive method [10] due to its superior resolution [7]. The majority of angular dispersive systems also rely on a known sample position to correctly interpret the diffraction pattern. We have been investigating a new technique which determines the sample location without the use of collimation. This has the capacity to speed up screening times as a whole depth dimension can be evaluated simultaneously. Efforts have also been made to consider the impact of sample thickness, which is known to be problematic in transmission mode [8,10]. This preliminary study demonstrates a small scale system that utilises molybdenum radiation. The penetrating ability of this radiation is at the lower limit for letter or parcel screening and certainly too low to penetrate a full suitcase. Typically for higher penetration imaging, airports may employ a tungsten target with a characteristic line at approximately 59 keV. This radiation comes with a penalty of increased Bremsstrahlung. However the use of appropriate K edge filtration would mitigate against this effect and so theoretically the techniques presented here could be used with tungsten radiation in a scaled up version. K edge filtration would also come with the additional benefit that it will improve the image quality of transmission based imaging systems..

### 1.1 Principles of X-ray diffraction

The majority of illicit materials such as explosives and drugs are polycrystalline and so a powder diffraction model has been adopted. Diffraction maxima occur when a mono-energetic X-ray beam strikes a crystalline material (or any material exhibiting long range order) at a specific angle of incidence. Constructive and destructive interference effects result in radiation being scattered at characteristic angles [11]. These are directly related to the differing interplanar spacings within the material. This relationship is governed by Braggs law,

$$\lambda = 2ds\sin\theta \quad (1)$$

where  $\lambda$  is the wavelength of the radiation used,  $d$  is the interplanar spacing within the material and  $2\theta$  is the angle through which the radiation is scattered relative to the incident beam direction. Thus if monochromatic radiation is used and the angle of scatter for any Bragg peak measured, then the interplanar spacings (characteristic of material) can be determined. Clearly the sample position relative to the detector is a critical factor for calculating the angle of scatter in most experimental systems. We have been developing a new approach which does not require a prior knowledge of sample position.

## 1.2 Rationale

Consider a diffraction pattern consisting of multiple diffraction maxima collected on a planar detector arranged normal to the incident beam (see figure 1). Translating the detector along the primary beam, will result in the Bragg maxima striking the detector at different locations i.e. the radius of the Debye cones` projection onto the detector (H) will change. The angle of scatter for each Bragg peak can thus be calculated from,

$$dH/dP = \tan 2\theta \quad (2)$$

where P is the sample to detector distance. Therefore, by measuring the rate at which the radius changes as the sample to detector distance is changed, it is possible to determine both the scatter angle and the sample position (relative to the detector) simultaneously. In principle then a minimum of two diffraction patterns need be measured in order to determine both  $2\theta$  and the sample position. However in practice this is not possible, particularly in the case of measured diffraction patterns consisting of multiple Bragg peaks as there is no reliable coincidence information that can be used to identify the common maxima between each pattern. We have developed a method for correctly identifying such corresponding Bragg peaks ("peak tracking") and this is discussed below. It should be noted that peak amplitude is an unreliable characteristic to exploit in this context due to multiple factors affecting peak heights (e.g. overlapping maxima).

## 1.3 Peak Tracking

With no coincidence information, and assuming that all diffraction maxima (n) measured at one detector position are also observed at a second position, the number of possible Bragg peaks that could have created peaks in the observed detector positions ranges from  $(n(n + 1)/2)$  to  $n^2$ . Only a proportion of these Bragg peak possibilities will be correct. It is evident that for scenarios where n is large the proportion of correct Bragg peak possibilities to false will diminish. Our approach to identify corresponding diffraction maxima uses equation (2) applied to diffraction data collected from multiple ( $>2$ ) detector positions. The positions of any maxima are linearly related through the detector positions. Thus determining those peak positions which possess a fixed gradient when plotted against detector position enables coincidence grouping of the peaks. A correct d-spacing and source position may then be determined.

For non-ideal conditions (e.g. where diffraction peaks have a finite width and thus peak overlapping is more frequent), a greater number of detector positions may be required. The inclusion of additional detector positions will increase the specificity of the system, however it will also warrant either a higher associated system cost (for the additional detectors) or an extra time constraint (where the detector is moved to different positions). We have found that four detector positions will eliminate enough false Bragg peaks to differentiate simple volumes containing few materials. For complex volumes that contain  $>5$  materials with low symmetry the technique may require more than four detector positions to achieve high levels of sensitivity (true positive rate) and 1-specificity (false positive rate).

## 2. Method

### 2.1 Simulation

A simulation was created in Matlab® to demonstrate the premise of the peak tracking method and to aid in selecting possible configurations prior to experimental tests. A number of materials of a chosen thickness (elongation) were randomly assigned a position along the X-ray beam path within a boundary representing an imaginary inspection volume. The diffraction patterns for each material were then projected onto detectors at specified distances and linearly summed. It should be noted that the projected pattern from each material contributed equally to the resulting patterns at each detector position and no allowances for the scattering cross sections of the materials, re-absorption effects or preferred orientation were made. However, these factors only affect peak amplitude not position. Each of the 1D patterns were smoothed using a Savitzky-Golay filter, normalised and then a modified first differential was applied to provide a robust peak finder in the presence of noise. Finally, each pattern was evaluated to find potential correct 2θ solutions and their associated position on the primary X-ray beam path, the result of which is reported in section 3.1.1.

To test the robustness of the system a mixture of illicit material diffractograms (e.g. TNT, PETN) were evaluated in the presence of those from benign materials (e.g. talcum powder, sucrose). The diffraction patterns produced by the peak tracking method were checked by a simple algorithm that searched a limited threat database of diffraction patterns to determine if an illicit material was present. Receiver operator characteristic (ROC) curves were created to compare the true positive (sensitivity) and false positive (1 – specificity) rates. This demonstrates how often threats were correctly identified and how often benign materials are identified as a threat (false alarm) respectively. The number of Bragg peaks matching those of a threat material was used as the discriminating threshold to produce the ROC. A summary of these results can be found in sections 3.1.2 and 3.1.3. The reader may be interested in the false negative rate (e.g. how often the system fails to identify a threat). This is 1 – true positive rate.

### 2.2 Experimental parameters

We have undertaken a systematic series of experiments incorporating samples placed at different distances from a detector and resultant diffraction patterns collected at increasing sample to detector distances. The X-rays were produced by a Philips PW1830 X-ray generator incorporating a sealed, long fine focus X-ray tube with a molybdenum target. The accelerating voltage and current were 40kV and 30mA respectively. A PIXIS 1024x1024 16bit CCD camera with a phosphor screen was used in a raster scan mode to collect the scattered photons. A 4mm thick brass plate with 0.66mm diameter aperture was used to collimate the primary X-ray beam into a pencil beam. Finally, a set of Thorlab stages were used to translate the detector along the primary beam path.

## 2.3 Materials

In the example shown in section 3.2, sheet aluminium (approximately 0.2mm thick) and aluminium oxide (approximately 0.1mm thick) were used as they present characteristic diffraction maxima over a typical angular range. Relatively thin samples were chosen due to the low energy X-rays employed as well as its subsequent affect on Bragg maxima width (presented in section 3.1.2 and discussed in section 4). In addition, these two materials are chosen as it would be difficult to differentiate between them by applying elemental techniques, which helps to demonstrate the specificity achievable with a scatter based system.

## 3. Results

### 3.1 Simulations

#### 3.1.1 The premise

Figure 2 illustrates the simulated patterns created from a spatially separated mixture of trinitrotoluene (TNT) and talcum powder (each at 0.1 mm elongation) when viewed at differing detector positions. The change in peak position ( $\Delta H$ ) is a function of  $2\theta$  and the materials' position along the primary X-ray beam path. Applying the peak tracking method described in section 1.3 results in many possible calculated  $2\theta$  values and positions. Two of these groups of Bragg peaks are demonstrated in figures 3 and 4. The peak positions were a good match to those of standard TNT and talcum powder proving to be the most likely candidate as determined by a conventional diffraction matching algorithm (Crystallographica Search-Match®) that searched approximately 200,000 diffraction patterns. Thus, from a mixture of diffraction patterns arising from differing sample positions, the algorithm was capable of discriminating between materials and locating their relative positions with respect to the detector.

#### 3.1.2 Effect of elongated samples

The peak tracking method is dependent upon the algorithm's ability to correctly identify peak positions at the detector. When samples are elongated along the primary beam axis the diffraction patterns, when collected in transmission mode, are known to be problematic. This is because broadening in the diffraction maxima caused by scattering from the front surface right through to the back surface of the sample is observed [10]. This reduces the precision in peak location and increases the overlapping likelihood. Figure 5A illustrates the change in shape of an ROC curve as the samples under inspection are elongated. Each individual simulation contained two materials (chosen at random from a small reference library of benign and illicit materials) at a specified elongation assigned to a random location within the inspection volume. Theoretical detectors were placed at 210, 220, 230 and 240 mm from the source. The ROC curve demonstrates the systems ability to reliably identify a threat material. The number of peaks required to identify the threat was used as the discriminating threshold. The

simulation was repeated approximately one thousand times. The results of this simulation are discussed in section 4.0.

### 3.1.3 Effect of detector distance

Increasing the sample to detector distance could mitigate against the reduced resolution offered by elongated samples. This is because the concomitant increase in relative diffraction peak width would be less than that of the corresponding positional change. Similarly to figure 5A (described in section 3.1.2), figure 5B illustrates an ROC surface with the same simulation settings except the detector distances were increased from 210, 220, 230 and 240 mm to 220, 240, 260 and 280 mm. The change in volume bounded by the surface is discussed in section 4.0.

### 3.2 Experimental proof of principle

To evaluate the methods empirically sheets of aluminium and aluminium oxide were placed at different locations along the primary beam path to simulate objects at differing locations in a volume. The diffraction patterns were then measured at four different detector positions relative to the inspection volume. The intensities within each pattern were radially integrated to produce the 1D scattering patterns illustrated in figure 6. It should be noted that evaluating thin samples with large crystallites can result in incomplete Debye rings. Radially integrating the pattern from a 2D detector mitigates against this effect.

Similarly to that demonstrated in section 3.1.1 the Bragg maxima recorded at each detector position were evaluated to identify those with behaviour consistent with equation 2. The results are illustrated in figures 7 and 8. These patterns correspond well to those produced by aluminium and aluminium oxide. Some of the standard peaks from aluminium and aluminium oxide are missing in the tracked patterns; this effect is caused by the peak overlapping phenomenon mentioned previously. An additional compounding consideration is that any preferred orientation affects may cause peak amplitudes to diminish below the noise level of the detector.

## 4. Discussion and Conclusion

A novel and versatile rationale capable of identifying the angles of scattered radiation ( $2\theta$ ) as well as the positions of diffracting materials (sample position) has been proposed and validated in the laboratory. The technique would lend itself well to the characterisation of materials within a volume such as those required in an airport screening environment because a prior knowledge of the sample position is not required. Multiple unknown materials that are spatially separated along the primary X-ray beam path can also be resolved simultaneously. Therefore, it could be used to increase the efficiency of mail screening systems as multiple letters (located at differing depth planes) could be evaluated at once. Perhaps one of the more interesting aspects of this technique is that the spatial differentiation is achieved without the use of post-sample collimation. Such collimation can result in a loss of as much as 99% of the scattered beam flux

(Malden and Speller, 2000) and such systems are thus inherently inefficient. Another related consideration is the approach in deriving the sample position. For systems that use post-sample collimation, the sample position is at the point of intersection defined by the primary and diffracted beam collimators. As such the precision to which the sample position can be identified is constrained by the engineering and mechanical tolerances of the collimators. Our approach has no such limitation.

One of the main confounding factors of this technique is that of samples elongated along the primary beam. If the sample(s) are elongated along the primary beam axis then in transmission diffraction maxima broadening is observed. This impedes the performance of the peak tracking method. The extent to which the performance is affected is illustrated by the ROC surface figure 5A. As the samples are elongated the ROC flattens nearing the no-discrimination line. To combat the loss in resolution introduced by elongated samples section 3.1.3 evaluates the idea of increasing the sample to detector distances. The rate at which the Debye cone propagates with respect to P is greater than the diffraction maxima broadening introduced by the diverging pencil beam. For this reason increasing the sample to detector distances acts as a positive optical lever. The result of increasing the sample to detector distance is seen best in figure 5B. ROC curves are compared typically using their respective areas. As we are evaluating a third variable (elongation) it is appropriate to compare the respective volumes bounded by the ROC surfaces, where a volume of 100% would provide perfect discrimination and 50% would provide no discrimination. Figure 5A has a volume of 84% whereas figure 5B has a volume of 89%. We therefore infer that increasing the sample to detector distances should help alleviate some of the issues encountered by elongated samples. Further, such increases in physical dimensions may well be a natural requirement for some applications of our technique. This preliminary work is part of an ongoing programme to incorporate X-ray diffraction based materials discrimination into an imaging technique. As a next step we intend to combine this approach with the novel tomographic approach afforded by kinetic depth effect X-ray imaging [12].

### Acknowledgments

This ongoing programme of work is funded by EPSRC and is in collaboration with the UK Home Office Scientific Development Branch (HOSDB) and the US Department of Homeland Security (DHS).

### References

- [1] J. Yinon, Counterterrorist Detection Techniques of Explosives. Elsevier, Amsterdam, 2007.
- [2] G. Harding, Applied Radiation and Isotopes. 67 (2009) 287-295.
- [3] R. Speller, Radiation Physics and Chemistry. 61 (2001) 293-300.

- [4] C.H. Malden, R.D. Speller, Nuclear Instruments and Methods in Physics Research Section A. 449 (2000) 408-415.
- [5] R.D. Luggar, J.A. Horrocks, R.D. Speller, R.J. Lacey, Applied Radiation and Isotopes.48 (2) (1997) 215-224.
- [6] B. Sun, M. Li, F. Zhang, Y. Zhong, N. Kang, W. Lu, J. Liu, Microchemical Journal. 95 (2010) 293-297.
- [7] E.J. Cook, J.A. Griffiths, M. Koutalonis, C.Gent, S. Pani, J.A. Horrocks, L. George, S. Hardwick, R. Speller, Proc of SPIE. Vol 7310 (2009).
- [8] S. Pani, E. Cook, J. Horrocks, L. George, S. Hardwick, R. Speller, IEEE TRANSACTIONS ON NUCLEAR SCIENCE. 56 (2009) 1238:1241.
- [9] E. Cook, R. Fong, J. Horrocks, D. Wilkinson, R. Speller, Applied Radiation and Isotopes. 65 (2007) 959-967.
- [10] A. Dicken, K. Rogers, P. Evans, J. Rogers, J.W. Chan, Applied Radiation and Isotopes. 68 (2010) 439 – 443.
- [11] B.D. Cullity, Elements of X-ray Diffraction, Addison-Wesley Publishing Company Inc, 1956.
- [12] J.P. Evans, Y. Yui, J.W. Chan, D. Downes, Pattern Recognition Letters. 27 (2006) 1863 -1873.

**Figure captions**

**Figure 1.** The geometry of the X-ray diffractometer with four detectors superimposed at different positions along and normal to the primary X-ray beam path.

**Figure 2.** Simulation of the diffraction patterns observed on a series of linear arrays arranged normal to the primary X-ray beam path at 210, 220, 230 and 240mm from the source when spatially separated samples of TNT and talcum powder are placed in the beam.

**Figure 3.** Plot of a grouping of Bragg peaks tracked through the patterns illustrated in figure 2 believed to have a common origin. The pattern corresponds well with TNT.

**Figure 4.** Plot of a grouping of Bragg peaks tracked through the patterns illustrated in figure 2 believed to have a common origin. The pattern corresponds well with Talcum powder.

**Figure 5.** Surface A illustrates the change in shape of the ROC curve with elongation of the sample materials. Simulated detectors were placed at 210, 220, 230 and 240 mm. Surface B illustrates the same arrangement except the simulated detectors were placed at 220, 240, 260 and 280mm.

**Figure 6.** Radially integrated diffraction patterns of spatially separated aluminium and aluminium oxide measured normal to the primary beam at specified distances along the primary beam path.

**Figure 7.** Plot of a grouping of Bragg peaks tracked through the diffraction patterns illustrated in figure 8 which are believed to have a common origin. The pattern corresponds well with aluminium.

**Figure 8.** Plot of a grouping of Bragg peaks tracked through the diffraction patterns illustrated in figure 8 which are believed to have a common origin. The pattern corresponds well with aluminium oxide.

Figure 1

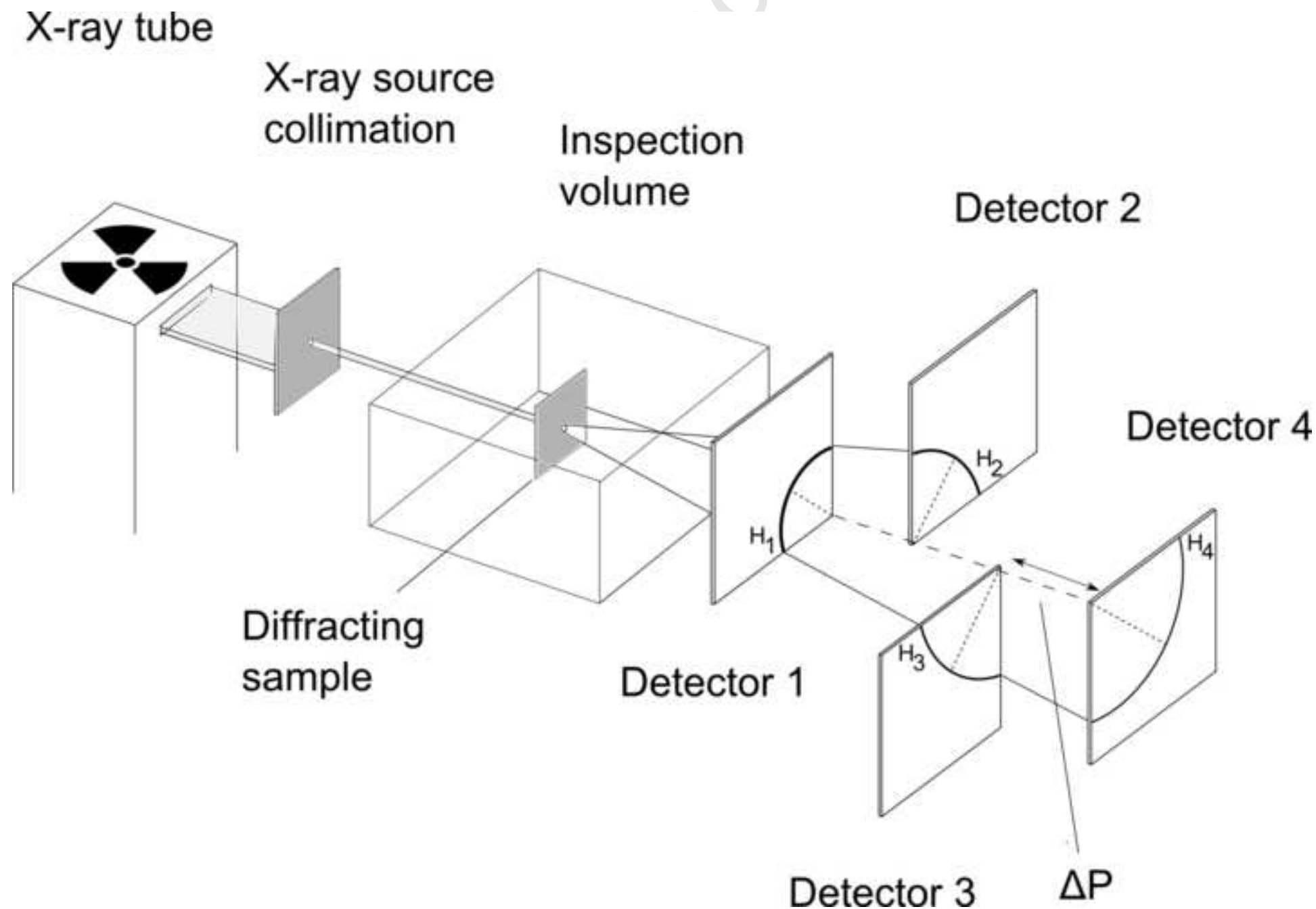


Figure 2

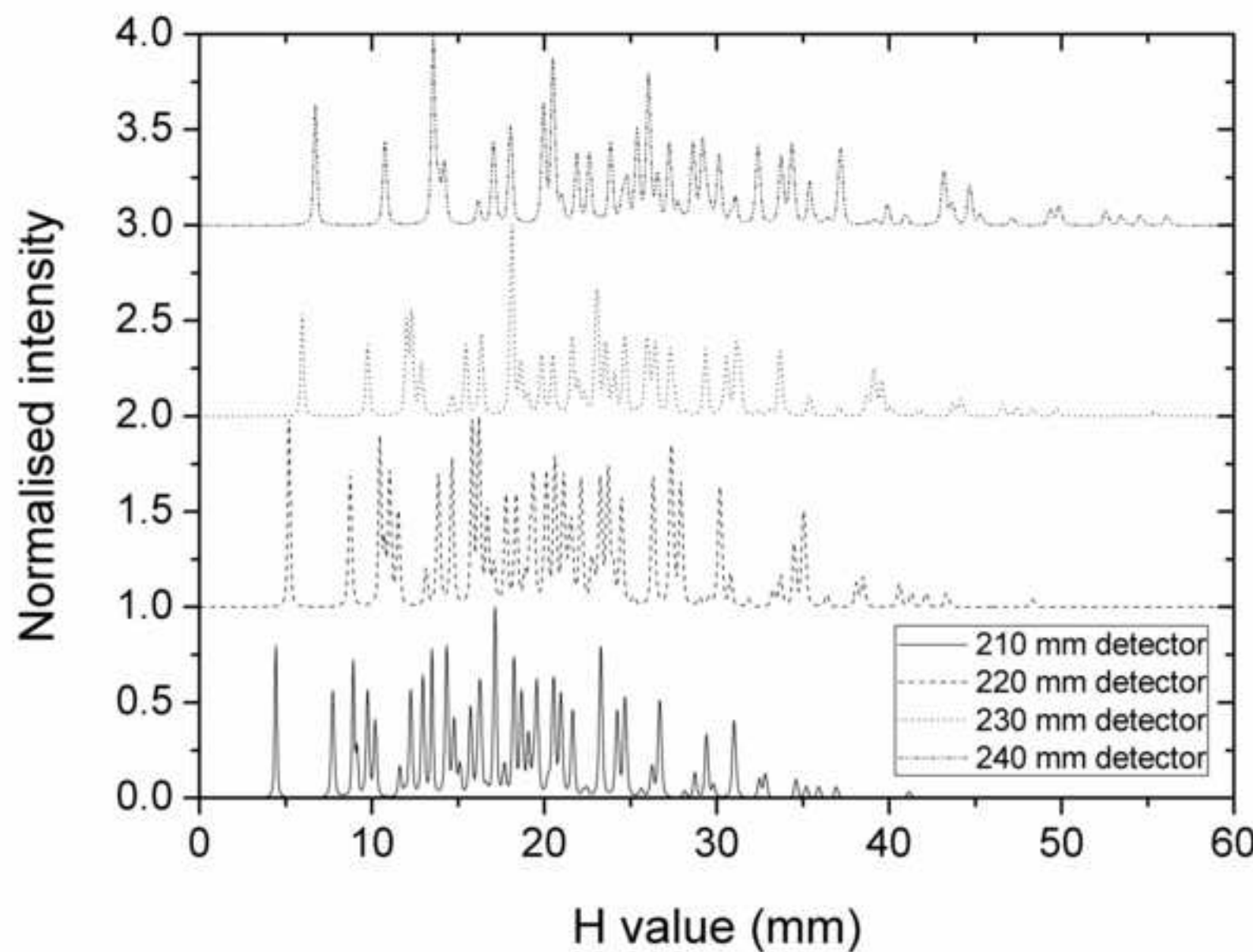


Figure 3

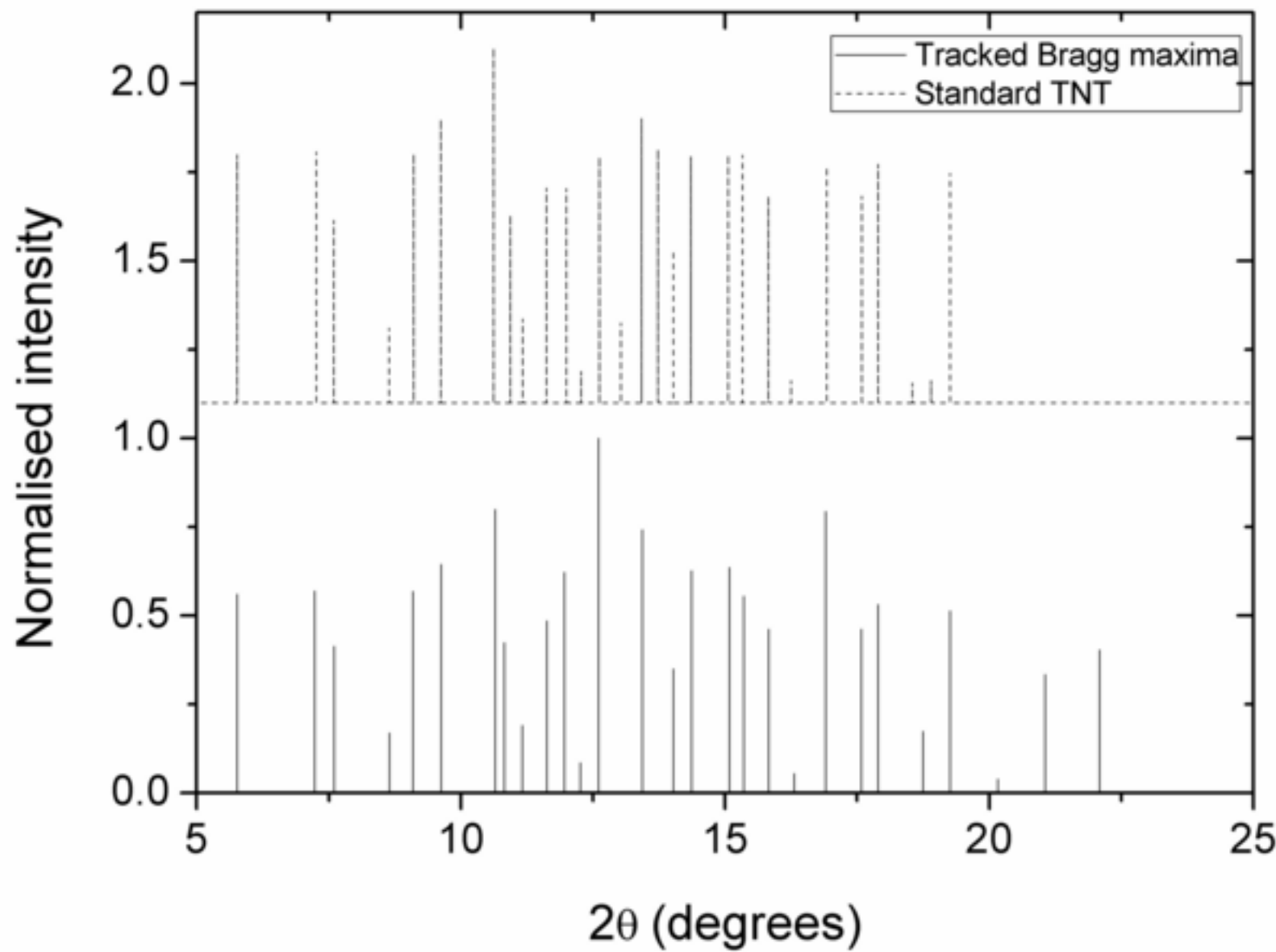
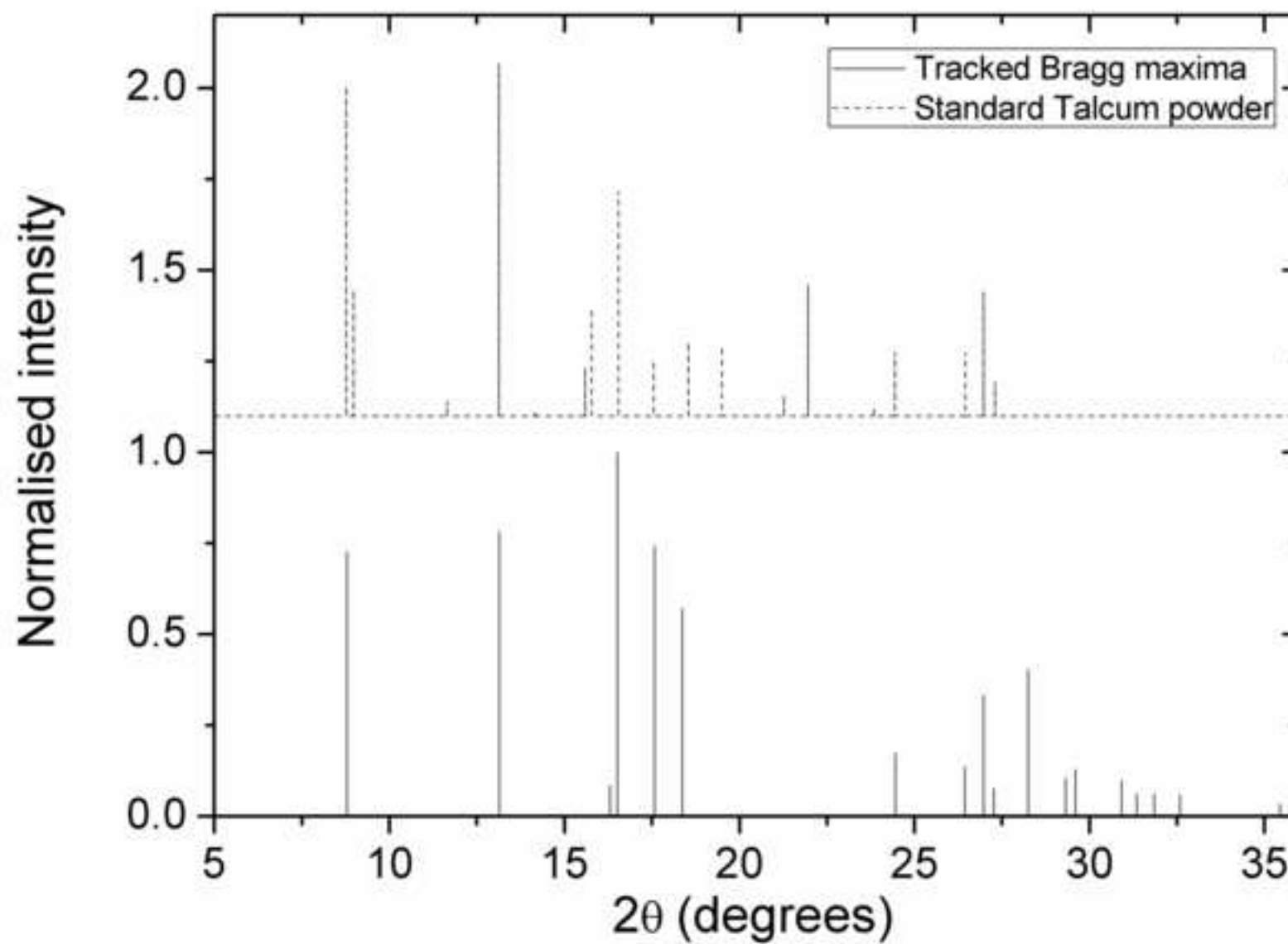


Figure 4



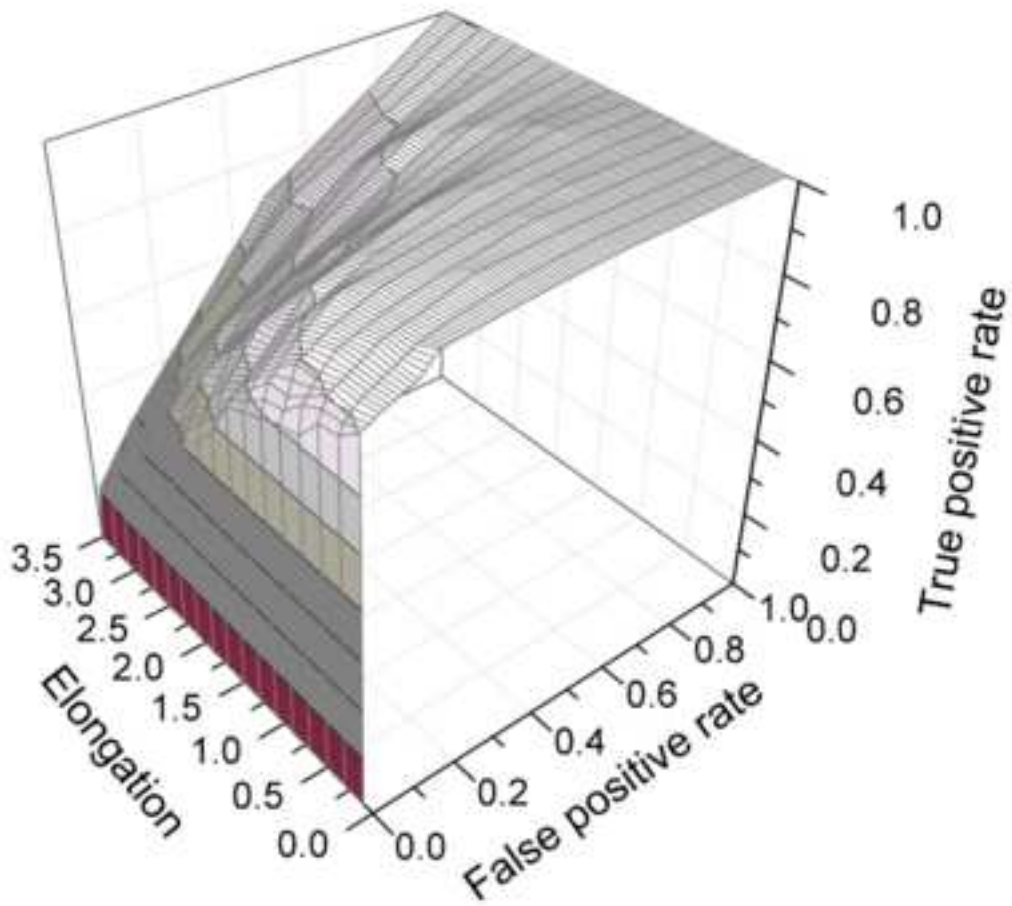
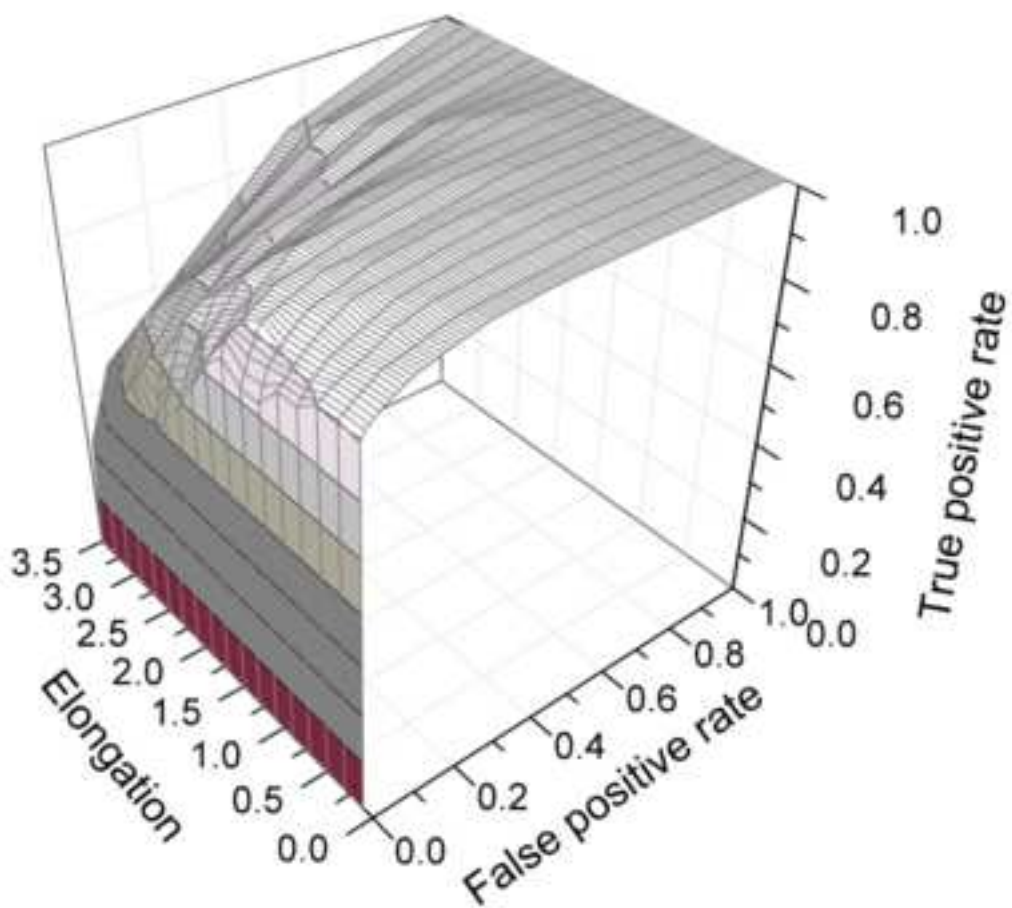
**A****B**

Figure 6

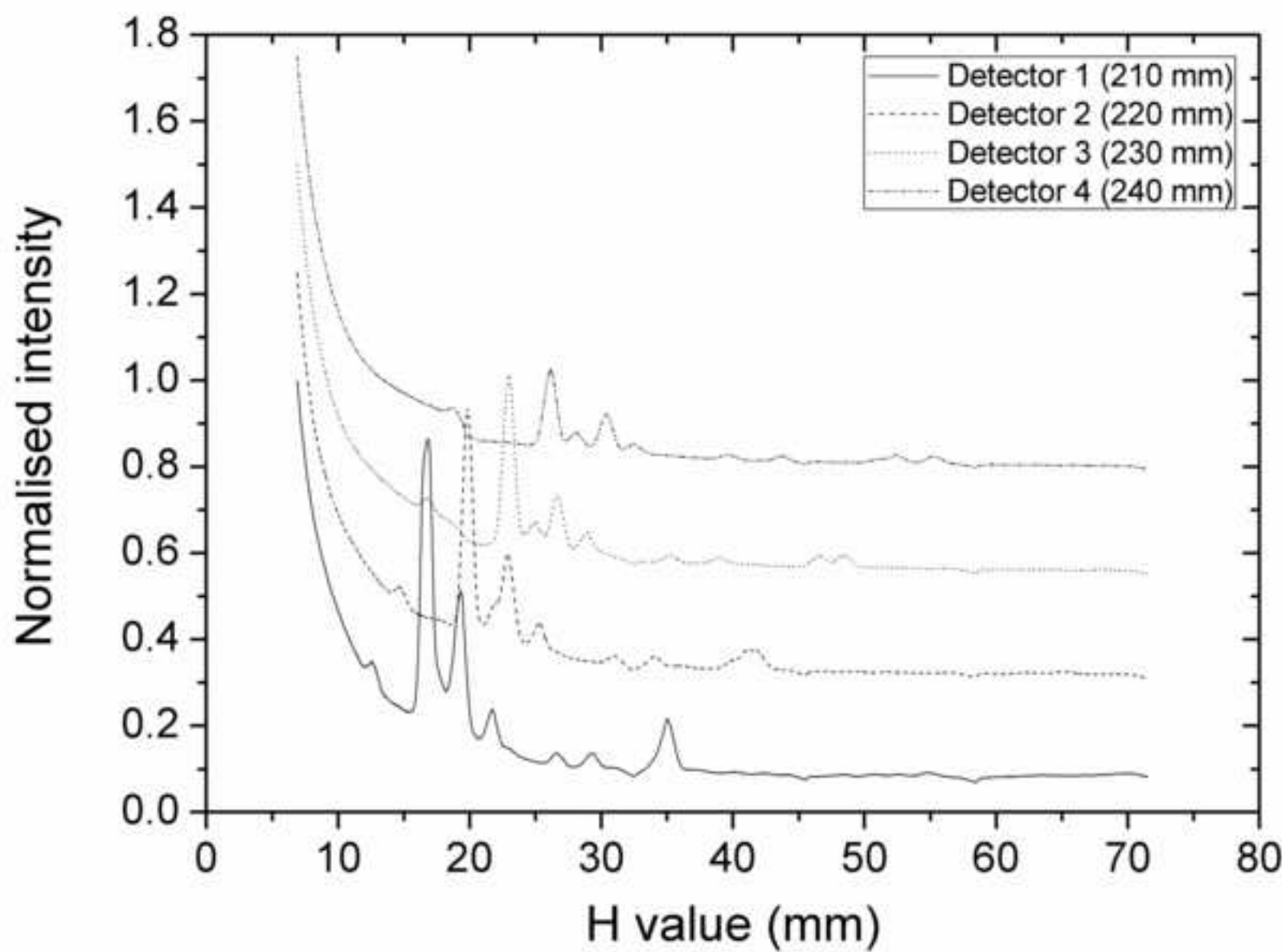


Figure 7

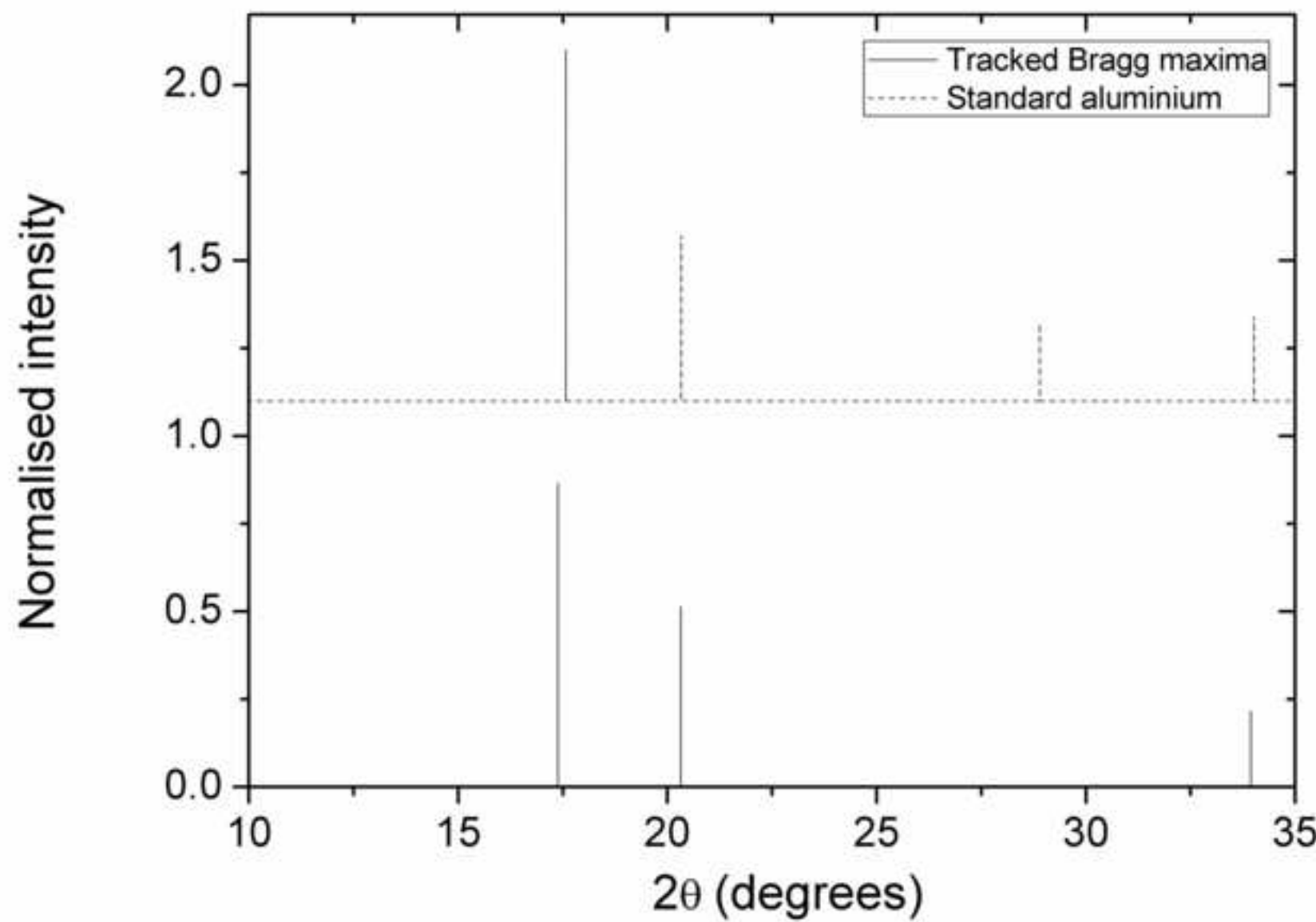


Figure 8

